https://doi.org/10.1016/j.renene.2020.11.132 **This is the Pre-Published Version.**

Techno-economic assessment of performance-enhanced parabolic trough receiver in concentrated solar power plants

Qiliang Wang [1, *], Gang Pei [2], Hongxing Yang [1, *]

[1] *Renewable Energy Research Group (RERG), Department of Building Services Engineering, The Hong Kong Polytechnic University, Hong Kong, China*

[2] *Department of Thermal Science and Energy Engineering, University of Science and Technology of China, Hefei 230027, China*

* Corresponding author. E-mail address: hong-xing.yang@polyu.edu.hk; qiliang.wang@polyu.edu.hk

Abstract

Solar-to-thermal conversion efficiency of the parabolic trough collector significantly degrades at high operating temperatures, which exerts seriously negative effects on the development of parabolic trough collectors. To solve this knotty problem, based on the theory of the negative thermal-flux region, a novel parabolic trough solar receiver with a radiation shield was proposed, manufactured, and tested. In this framework, the proposed solar receiver is employed in the concentrated solar power plants using solar salt as the heat transfer fluid to analyze its feasibility in real solar power plants. In this study, the mathematical models of heat collection and economic assessment are established, and the simulation results yield a good agreement with the experimental data. The techno-economic performances of the solar power plants installing the proposed solar receivers in three typical areas under different installed capacities and thermal storage capacities are comprehensively investigated. The results demonstrate that the proposed solar receiver has a great potential for significant enhancement of the techno-economic performance of the solar power plant. The

solar power plant with the proposed solar receivers located in Dunhuang can effectively improve the annual net electrical energy production by 9.77 %, reduce the levelized cost of energy by 8.67 %.

Keywords: *Parabolic trough collector (PTC); Solar receiver; Concentrated solar power (CSP); Techno-economic; Efficiency*

Nomenclature

a	Ambient
c	Specific heat capacity, J/(kg·K)
d	Discount rate
f	fluid
g	Glass envelope
h	Convection heat transfer coefficient, W/(K·m^2)
m	Mass flow rate, kg/s
s	Absorber tube
A	Area, m^2
C	Friction coefficient
D	Diameter, mm
E	Electricity
L	Length, m
Q	Net heat flux, W
T	Temperature, °C
W	Width, m
ap	Aperture
γ	Coefficient
θ	Angle, °
τ	Transmittance
α	Absorptance

Abbreviation and subscripts

ANI	Aperture normal irradiance, W/m^2
CSP	Concentrated solar power
DNI	Direct normal irradiance, W/m^2
FH	Fossil/heater expenditures
HL	Heat loss
HTF	Heat transfer fluid
kWe	Kilowatt of electricity
kWt	Kilowatt of thermal energy
kWhe	Kilowatt-hour of electricity
kWht	Kilowatt-hour of thermal energy
MWe	Megawatt of electricity
LCOE	Levelized cost of energy
NTR	Negative thermal-flux region

conv	Convection	OM	operation and maintenance costs
in	Inlet	PTC	Parabolic trough collector
out	Outlet	PTR	Parabolic trough receiver
Nu	Nusselt number	RMSD	Root-mean-square deviation
Re	Reynold number	RP	Relative percentage, %
Pr	Prandtl number	RS	Radiation shield
Greek Symbols		PTCSP	Parabolic trough CSP
η	Efficiency	SCA	Solar collector assembly
φ	Incidence angle, °	SSC	Solar selective-absorbing coating

1. Introduction

With great development of industrialization all over the world, the demands for hotter and larger amount of high-temperature heat source grows quickly. To date, the generation of heat source mainly relies on the combustion of fossil fuel [1], however, the incurred environmental pollution by the combustion of fossil fuel and impending energy crisis promote the mankind to focus more on the renewable energy applications. Concentrated solar thermal technologies, after almost four decades of great progresses, achieve great successes in commercial application of concentrated solar power (CSP) [2-5]. Parabolic trough collector (PTC) is the most widely used system among the concentrated solar thermal technologies due to its technical maturity and performance stability [6-9]. According to the statistics by the end of 2019, the total installed capacity of global CSP reached 6.59 GWe, and the parabolic trough CSP (PTCSP) accounts for above 80 % [10].

As a such promising system, however, the PTC system faces a knotty problem of deteriorating solar-to-thermal conversion efficiency at high operating temperature, which exerts seriously negative impacts on the further development and utilization of the PTC system. At present, the PTC system employed in CSP generally

uses therminol oil (VP-1) [11, 12] as the heat transfer fluid (HTF) in commercial utilization, the operating temperature of PTC system is approximately 400 °C while the efficiency of a steam turbine is only 36-38%. To improve the steam turbine efficiency and storage temperature in CSP, the HTF of solar binary salt is considered and applied to the PTC system so that the operating temperature is enhanced to 550 °C [13]. The corresponding turbine efficiency increases to approximately 40 %. At such high operating temperatures of 400 °C even 550 °C, parabolic trough solar receiver (PTR), as the key component of PTC system where solar-to-thermal conversion process occurs, generates massive heat loss [14], that results in the strong decrease of the solar-to-thermal conversion efficiency of PTC system.

Conventional PTR is mainly composed of metal absorber tube deposited with solar selective-absorbing coating (SSC), glass envelope, metal-glass sealings [15, 16]. The annulus between the absorber tube and glass envelope is evacuated for the effective blockage of convection and conduction heat loss from the absorber tube, thereby the heat loss of PTR is basically equivalent to the radiation heat loss. According to the Stefan-Boltzmann's law [17], the radiation heat loss from the absorber tube considerably increases with the absorber temperature raised to the fourth power. In a Eurotrough collector [18] installing Schott's 2008 PTR70 parabolic trough receiver [14], for instance, in the case of normal solar irradiance of 600 W/m^2 and absorber temperature of 400 °C, the radiation heat loss of the PTR accounts for almost 10.0 % of absorbed solar irradiance by the PTR [14], which exerts a seriously negative impact on the solar-to-thermal conversion efficiency of PTC system. Therefore, the effective reduction of radiation heat loss of PTR at high operating temperatures is vital for improving the solar-to-thermal conversion efficiency of the PTC system. Lowering the infrared emittance of SSC on the surface of the absorber tube is the most effective way to reduce the radiation heat loss of PTR [19, 20]. However, the solar irradiance absorptance of SSC would suffer much and thus leading to a large amount of solar irradiance loss due to a high concentration ratio (>80) in the PTC system. Therefore, this

optimization method for SSC may instead cause a decrease in thermal efficiency of the PTC system. Besides of this method, Osorio et al. [21] proposed a new PTR with double glass envelopes, McEnaney et al. [22] used aerogels instead of vacuum gap of PTR, these methods can effectively reduce the radiation heat loss from the absorber tube, but they also caused the reductions in transmittance of solar irradiance to reach absorber tube surface, thereby the thermal efficiencies of the proposed PTRs were hardly enhanced in the PTC system with high concentration ratio.

Unlike the optimization methods mentioned above, we proposed a novel PTR with a radiation shield placed in the vacuum gap based on the theory of the negative thermal-flux region (NTR) [23, 24]. As exhibited in Fig. 1, a standard commercial PTR in EuroTrough collector absorbs high concentrated solar irradiance (80×) at the lower part, but the nonconcentration part of PTR with the angle range of 290~360(0)~70° only absorbs no more than one solar irradiance (≤ 1×). In the case of solar irradiance of 600 W/m^2, the maximum absorbed solar irradiance in nonconcentration part is about 0.56 kW/m^2. According to the experimental results carried out by the NREL [14], the circumferential radiation heat loss from the absorber tube is calculated to be 3.05 kW/m^2 at the absorber temperature of 550 °C, which is approximately 5.4 times the absorbed solar irradiance by the absorber tube in noncencentration part. As shown in Fig. 1, larger radiation heat loss than the absorbed solar irradiance occurs on the absorber tube with the angle range of 275~360(0)~85°, resulting in the phenomenon of negative net heat gain and the formation of the negative thermal-flux region (NTR). Furthermore, it has been proven that the phenomenon of negative net heat gain in NTR will get worse at higher absorber temperature or lower solar irradiance [23]. The discovery of NTR has given rise to new optimization methods of PTR for the enhancement of thermal performance, i.e., structural optimization integrating functional materials for the NTR [25-28]. For instance, the SSC in the NTR was replaced with the polished metal layer which has extremely low emittance in the whole wavelength band [25]. The metal layer can greatly

reduce the radiation heat loss in the NTR but with losing nearly all of incident solar irradiance due to the low absorptance of metal layer, the results showed that the proposed PTR with double SSCs still possessed superior overall thermal performance at high operating temperature.

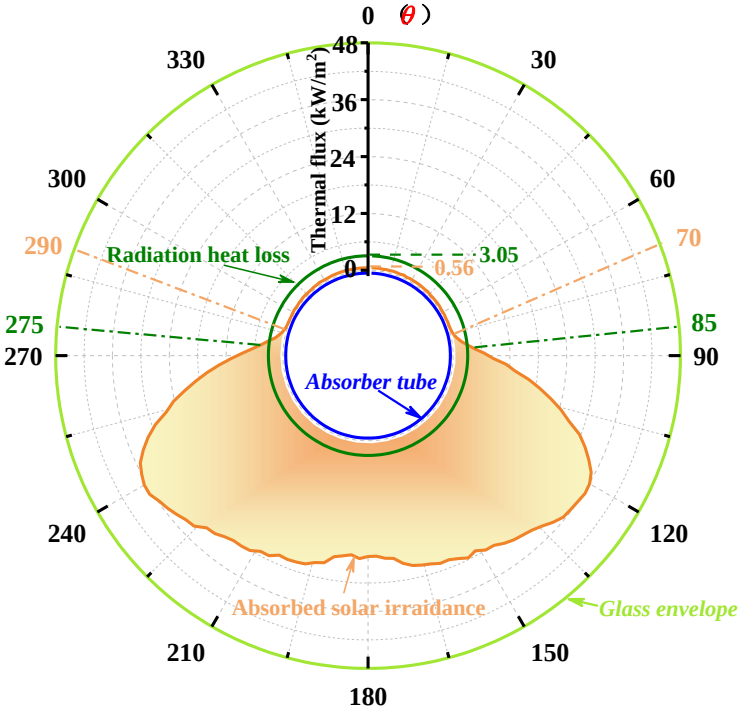

Fig. 1 Negative thermal-flux region (NTR) occurring in the upper part (angle range: 275~360(0)~85°) of PTR. In this part, the radiation heat loss from the absorber tube is obviously higher than the absorbed solar irradiance by the absorber tube at high absorber temperature or low solar irradiance, thereby forming the region with negative net heat gain.

Introducing a metal radiation shield (RS) into the vacuum annulus in the NTR is another effective and proven way to reduce the radiation heat loss and improve the solar-to-thermal conversion performance of PTR. The schematic diagram of the PTR integrating a RS (PTR-RS) is exhibited in Fig. 2. RS was made of aluminum, the inner aluminum surface of RS was polished to achieve high reflectance for the maximum blockage of radiation heat loss from the absorber tube, and the outer surface of RS was deposited with the SSC to enhance the RS temperature to reduce the radiation heat transfer between the absorber tube and the RS. The addition of RS can effectively reduce the radiation heat loss with incurred acceptable solar irradiance loss. Unlike the other novel PTRs proposed in references [25-28], the novel PTR-RS was systematically

designed and experimentally validated in small-scale testing platforms [29]. As shown in Fig. 3(b) and (c), the conventional PTR and novel PTR-RS were manufactured and tested in the indoor and outdoor small-scale testing platforms. In comparisons with the conventional PTR, it has been proven that the PTR-RS can achieve good structure reliability and superior solar-to-thermal conversion performance at the high temperature (303 °C@*DNI*=800 W/m^2) or low direct normal irradiance (*DNI*), but inferior performance at the lower temperature or higher *DNI*. In a real PTCSP plant system, however, not whole PTRs in a long solar field loop have high HTF temperature. The HTF temperature increases from the lower inlet temperature, which demonstrates the HTF temperature in the front part of the loop may be too low to achieve superior performance. Moreover, the values of *DNI* are variable in different regions and seasons. Therefore, the overall performance and feasibility of the proposed PTR-RS in a real PTCSP plant system need further verifications.

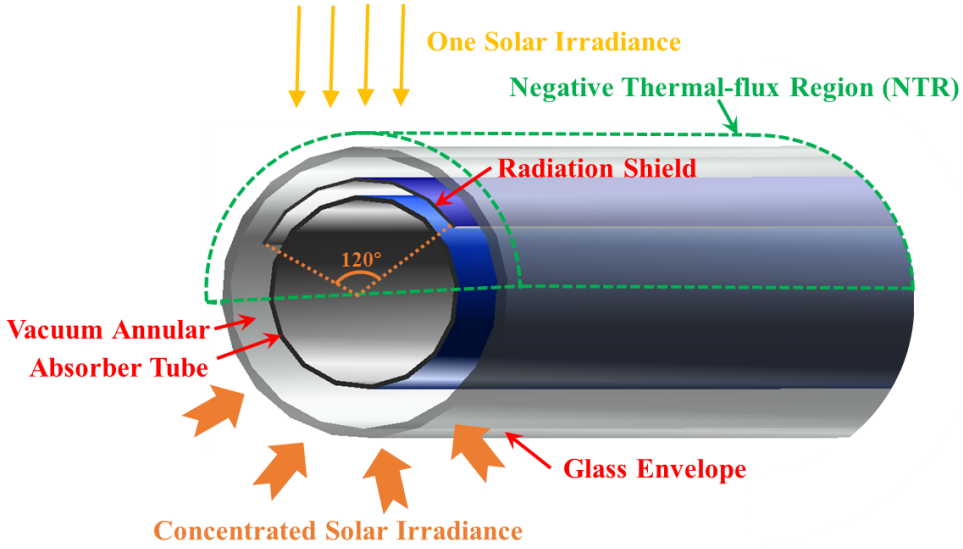

Fig. 2 Schematic diagram of the proposed PTR-RS.

In this study, 100 MWe PTCSP plant systems with the PTRs and PTR-RSs (Fig. 3(a)) are investigated. The PTCSP plants adopt solar binary salt [30] as the HTF, and the outlet HTF temperature of a single loop in the PTCSP plant is determined as 550 °C. In this framework, detailed mathematical models regarding the heat collection and economy of the PTCSP plants are established, thermal performances of PTCSP plant systems integrating the PTRs and PTR-RSs in the daytime and nighttime are evaluated. The impacts of different

regions, namely, Mojave Desert, Quarzazate, and Dunhuang, on the techno-economic performances of the PTCSP systems are also investigated to validate the feasibility of the PTR-RS in different regions. Furthermore, the technical and economic assessments and comparisons of the PTR-RS in the PTCSP with different installed capacities and thermal storage capacities are also carried out in detail.

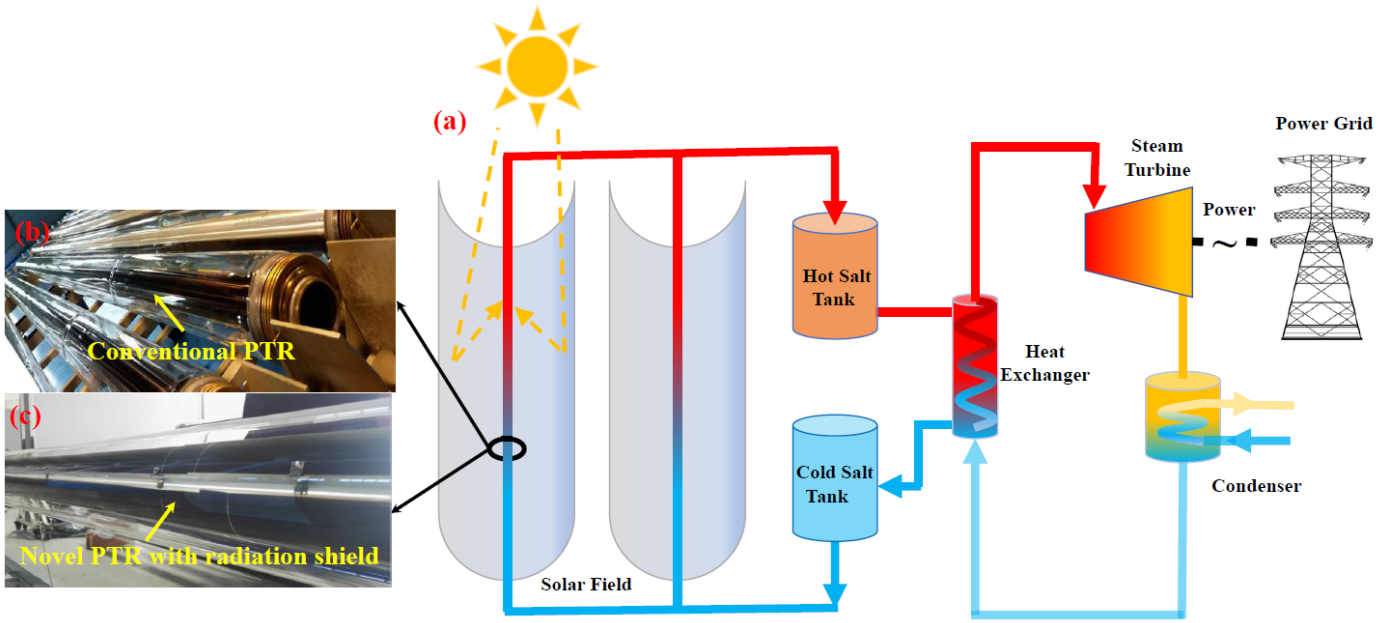

Fig. 3 PTCSP plant system using the solar binary salt as the HTF. (a) Schematic diagram of PTCSP system, (b) conventional PTR manufactured, and (c) novel PTR-RS manufactured.

2. Characteristics of PTCSP system

Due to the good thermo-physical characterization, low cost, and long life, solar binary salt is a promising HTF used in the CSP system. The binary salt is composed of 60 % $NaNO_3$ and 40 % KNO_3 (weight percent, %), the freezing temperature and the maximum operating temperature are approximately 238 °C and 593 °C, respectively [31]. The complete cycle of solar salt in the PTCSP system is exhibited in Fig. 3(a). The solar salt flows inside the solar receivers in the solar field to absorb the heat through a solar field loop. It then is pumped into the hot salt tank and exchanged by the heat exchanger for the steam used to drive the turbine. The heat-releasing solar salt eventually flows to the cold salt tank and is pumped into the solar field loops to complete a cycle.

2.1 Solar field

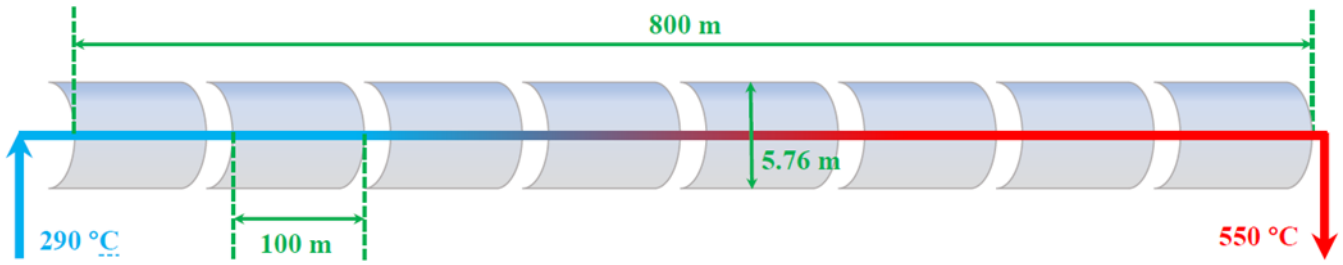

Fig. 4 Single solar field loop in the PTCSP system. The inlet and outlet temperatures of HTF are determined as 290 and 550 °C, respectively.

In this study, the solar field loops use the EuroTrough collectors with an aperture of 5.76 m [32], each loop has 8 solar collector assemblies (SCAs) as shown in Fig. 4. A SCA is an individually tracking component of the solar field that includes trough mirrors, receivers, and a supporting structure. All SCAs employ the orientation of North-South (N-S) on the type of single axis tracking of East-West (E-W), the spacing of each two rows is 15 m for reducing the shading by the front row. The detailed specifications of single solar field loop are presented in Table 1.

Table 1 The specifications of the single solar field loop [14, 29, 32]

Parameter	Specification	Parameter	Specification
Single SCA length	100 m	Row spacing	15 m
SCA number in single loop	8	Loop optical efficiency ($\eta_{0,\,PTR}$)	0.736
Single loop length (L_{loop})	800 m	Loop optical efficiency ($\eta_{0,\,PTR\text{-}RS}$)	0.724
Aperture width (W_{ap})	5.76 m	Length of solar receiver	4.06 m
Single loop aperture area (A_{ap})	4360 m^2	Diameter of absorber tube (D_s)	70 mm
Receiver number in single loop	192	Diameter of glass envelope (D_g)	125 mm
Loop inlet HTF temperature (T_{in})	290 °C	Diameter of RS in PTR-RS (D_{RS})	80 mm

Loop outlet HTF temperature (T_{out})	550 °C	Angle of RS arc in PTR-RS (θ_{RS})	120°

The loop inlet and outlet HTF temperatures are designed as 290 and 550 °C, respectively. The solar receiver in the solar field loop employs conventional PTR and PTR-RS manufactured by TRX Solar technology Co. Ltd [29], physical PTR and PTR-RS are exhibited in Fig. 3(b) and (c). It is noted that all specifications of the PTR manufactured are the same as these of the widely available commercially solar receivers. The RS arc angle in the PTR-RS is 120° to avoid the interception of the concentrating solar rays. The distance between the RS and absorber tube is 5 mm, given actual fabrication installation difficulties. The presence of the RS will cause the optical loss of solar irradiance projected onto the PTR in the NTR, thus the optical efficiency of the PTR-RS decreases to 0.724 from the 0.736 in the PTR. The detailed calculation process of the optical efficiency is explained in section 3.

2.2 Thermal Storage and power cycle

Besides of a good HTF in the solar field, the solar salt is also a widely popular working medium used to store the excessive thermal energy in the daytime. In this study, the temperatures of the hot salt tank and cold salt tank are 550 and 290 °C, respectively. Generally, larger thermal storage capacity in the CSP system means stronger continuous generating capacity in the nighttime, which is conducive to increasing annual power generating capacity but the initial investment to the CSP system will inevitably rise [33, 34].

The HTF volumes with specified thermal storage capacity can be calculated to ensure that the storage system can supply energy to the power block at its design thermal input capacity for the number of hours specified by the full load thermal storage hours variable. In terms of thermal storage for 6, 8, and 10 hours, the available HTF volumes in the storage tanks are approximately 7390, 9853, and 12316 m^3. According to the operational data in the empirical CSP plant, the cycle thermal efficiency of the steam turbine is set as 0.407. In this study, the installed capacity of PTCSP plant is designed as 100 MWe.

3. Models and experimental validation

3.1 Heat collection model

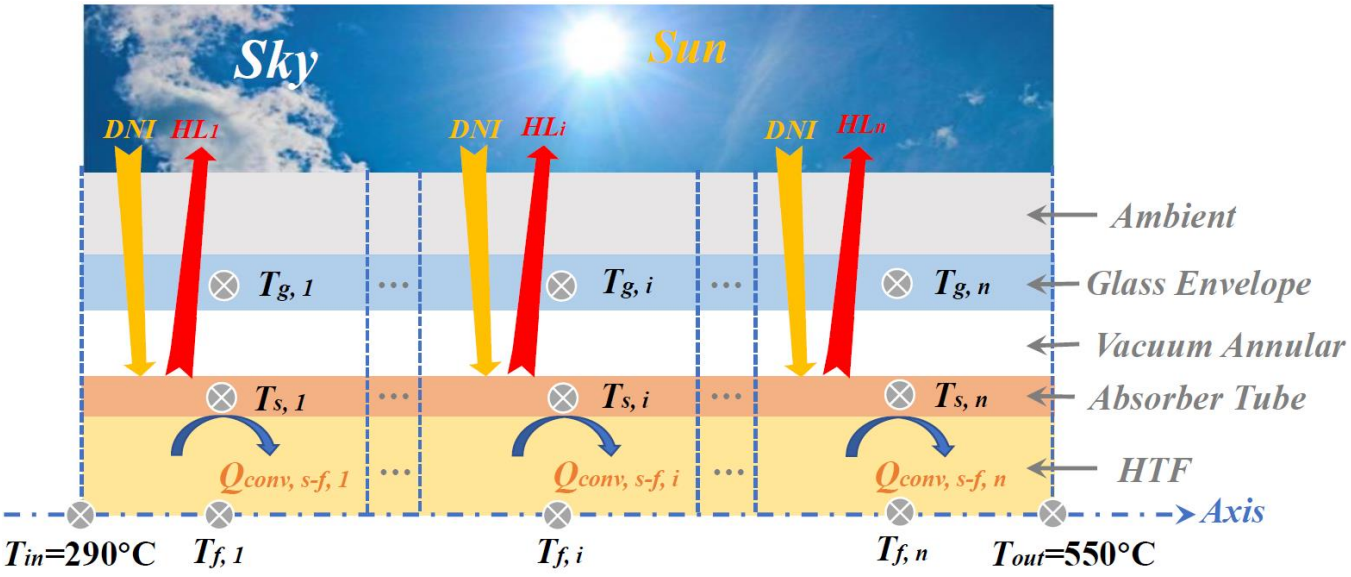

Fig. 5 The simulation of heat collection process by the finite volume method

As shown in Fig. 5, the steady-state heat collection process of a single solar field loop is simulated by the finite volume method. A uniform temperature distribution around the absorber tube is assumed. The heat loss and thermal efficiency of each solar field loop are two important indicators to observe the solar thermal performance of the solar receivers and PTC system. The heat loss (*HL*) of PTR and PTR-RS has been achieved by the indoor heat loss experiments (Fig. 7(a)). In actual application conditions, different environmental parameters, namely, ambient temperature, wind speed, and sky temperature, exert little effects on the amount of heat loss of PTR [14], thus it can be assumed that the heat loss of PTR or PTR-RS under different environmental parameters is the same at a determined absorber temperature. This framework employs the experimental heat loss results in the total heat loss and the heat collection simulations in a single solar field loop. The detailed heat loss experiments are presented in section 3.3. The fitting curves of experimental heat loss results of the PTR and PTR-RS used in the models are expressed as Eq (16) and Eq (17).

In the heat collection process, the single loop is divided into *n* finite volumes (*n*=800 in this study). In the

i^{th} finite volume (i=1, 2, …, n), the HTF temperature, absorber temperature, and glass envelope temperature are indicated as $T_{f,i}$, $T_{s,i}$, and $T_{g,i}$, °C. The values of $T_{f,i}$ and $T_{s,i}$ can be determined by iterative computations based on the energy balance in the i^{th} finite volume as expressed in Eq (1),

$$Q_{conv,s-f,i} + HL_i = \eta_0 A_{ap,i} \bullet ANI = \eta_0 W_{ap} L_i \bullet ANI \,, \tag{1}$$

where $A_{ap,i}$ is the aperture area of PTC corresponding to i^{th} finite volume, m^2; which is the product of aperture width (W_{ap}) and length of PTC loop in the i^{th} finite volume (L_i). HL_i represents the heat loss of PTT and PTR-RS in the i^{th} finite volume, W. ANI is the aperture normal irradiance, W/m^2, which is calculated by [35]:

$$ANI = DNI \bullet \cos\varphi \,, \tag{2}$$

where φ is the incidence angle of the direct normal irradiance (DNI), rad. η_0 in Eq (1) represents the optical efficiency of the PTC system in a single loop. The loop optical efficiency of the PTC system integrated with PTRs ($\eta_{0,\,PTR}$) can be calculated by the expressions as follows:

$$\eta_{0,\,PTR} = \frac{ANI \bullet W_{ap} L_{loop} \bullet \gamma_{block}\gamma_{tracking}\gamma_{reflect}\gamma_{dust}\gamma_{other}\tau_g\alpha_s}{ANI \bullet W_{ap} L_{loop}} = \gamma_{block}\gamma_{tracking}\gamma_{reflect}\gamma_{dust}\gamma_{other}\tau_g\alpha_s \,, \tag{3}$$

where γ_{block}, $\gamma_{tracking}$, $\gamma_{reflect}$, γ_{dust}, and γ_{other} refer to the blockage coefficient (support structures, etc.), the tracking deviation coefficient, the reflectance of mirrors without dust, the influencing coefficient on the PTR and mirrors incurred by the dust, and the other coefficient, their values are determined as 0.971, 0.985, 0.925, 0.955, and 0.945. τ_g and α_s are the solar transmittance of glass envelope and solar absorptance of the SSC, respectively; their values are 0.960. Thus, the value of $\eta_{0,\,PTR}$ is calculated as 0.736. Based on the Eq (3), the optical efficiency of the PTC system integrated with PTR-RSs ($\eta_{0,\,PTR\text{-}RS}$) can be obtained by:

$$\eta_{0,\,PTR\text{-}RS} = \frac{ANI \bullet (W_{ap} - W_{RS}\gamma_{install}) L_{loop} \bullet \gamma_{block}\gamma_{tracking}\gamma_{reflect}\gamma_{dust}\gamma_{other}\tau_g\alpha_s}{ANI \bullet W_{ap} L_{loop}} = \eta_{0,\,PTR}\left(1 - \frac{W_{RS}\gamma_{install}}{W_{ap}}\right), \tag{4}$$

where W_{RS} represents the effective width of the RS blocking the direct solar radiation, m. It can be calculated by:

$$W_{RS} = D_{RS} \bullet \sin(\theta_{RS} / 2), \quad (5)$$

where D_{RS} and θ_{RS} are the diameter of RS and the angle of RS surrounding around the absorber tube, their values are presented in Table 1. It is noted that γ_{install} in Eq (4) represents the installing deviation coefficient of RS in practice, which is determined as 1.36 in this study.

$Q_{conv,s-f,i}$ in Eq (1) refers to the heat transfer between the absorber tube and the HTF in the i^{th} finite volume, i.e., the net heat gain, W, which can be expressed as follows [36],

$$Q_{conv,s-f,i} = h_{conv,s-f,i} A_{s,i} (T_{s,i} - T_{f,i}), \quad (6)$$

where $A_{s,i}$ represents the inner surface area of absorber tube in the i^{th} finite volume, m^2. $h_{conv,s-f,i}$ is the convection heat transfer coefficient, W/(K·m^2), it is calculated by the expression as follows:

$$h_{conv,s-f,i} = \frac{Nu_{f,i} \bullet k_{f,i}}{L_i}, \quad (7)$$

where $k_{f,i}$ represents the HTF thermal conductivity in the i^{th} finite volume, W/(m·K). $Nu_{f,i}$ refers to the Nusselt number of the HTF in the i^{th} finite volume. For the full developed transitional and turbulent flow in circular ducts, the Nusselt number can be determined by the correlation given by Gnielinski [37]:

$$Nu_{f,i} = \frac{(C_{f,i}/2)(\text{Re}_i - 1000)\,\text{Pr}_i}{1 + 12.7 \bullet (C_{f,i}/2)^{1/2} (\text{Pr}_i^{2/3} - 1)}, \quad (8)$$

where $C_{f,i}$, Re_i, and Pr_i represent the friction coefficient, Reynold number, Prandtl number of the HTF in the i^{th} finite volume.

In the heat collection calculations of the one-loop PTC system integrated with PTRs, the initial fluid inlet temperature (T_{in}) is determined as 290 °C and used as the average fluid temperature ($T_{f,1}$) in the 1st finite volume. The iterative absorber temperature ($T_{s,1}$) in 1st finite volume is continuously substituted into the Eq (6) and Eq (16), the net heat gain of the fluid and net heat loss from the absorber tube can be thus calculated. Once the calculated values satisfy the law of energy balance in the absorber tube, which can be judged by

inequation (9), the correct absorber temperature, net heat gain, and net heat loss can be eventually achieved.

$$\left|Q_{conv,s-f,i} + HL_i - \eta_0 A_{ap,i} \bullet ANI\right| < 0.1 . \quad (9)$$

Subsequently, the outlet fluid temperature in the 1st finite volume, i.e., the fluid inlet temperature in the 2ed finite volume ($T_{f,2}$), can be calculated by Eq (10):

$$T_{f,i+1} - T_{f,i} = \frac{Q_{conv,s-f,i} L_i}{\dot{m} c_p} , \quad (10)$$

where c_p is the specific heat of the HTF, J/(kg·K). $\dot{m}$ represents the mass flow rate, kg/s. After the value of $T_{f,2}$ is calculated, the same calculations repeat from the Eq (6) for the heat collection process in the 2ed, 3rd, …, 800th finite volumes. The detailed computational flow chart is exhibited in Fig. 6.

After all heat collection processes in a single solar field loop, the total heat gain of the HTF through the solar field loop is achieved by accumulating all of the heat gains in involved finite volumes:

$$Q_{conv,s-f} = \sum_{i=1}^{n} Q_{conv,s-f,i} \ (n=800). \quad (11)$$

Similarly, the total heat loss of the solar receivers in a single loop can be calculated by:

$$HL_{loop} = \sum_{i=1}^{n} HL_i \ (n=800). \quad (12)$$

Therefore, the thermal efficiency of the single loop can be calculated by the expression [38]:

$$\eta = \frac{Q_{conv,s-f}}{ANI \bullet A_{ap}} = \eta_0 - \frac{HL_{loop}}{ANI \bullet A_{ap}} . \quad (13)$$

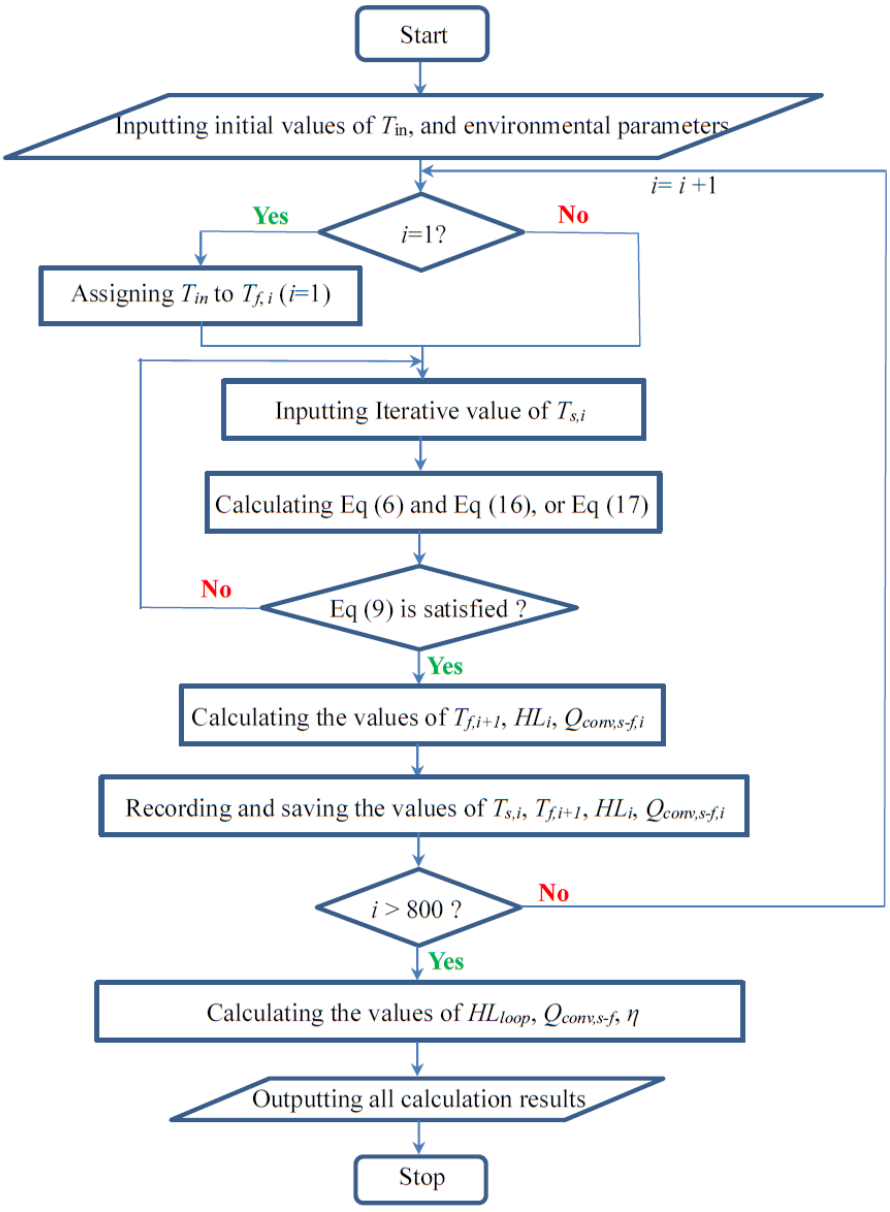

Fig. 6 Computational flow chart of heat collection models

3.2 Economic assessment strategy

To observe the economic performance of the PTCSP plant with the PTR-RS, an economic assessment strategy is constructed in this section. Generally, PTCSP system costs mainly consist of initial investment, operation, and maintenance costs. In this study, the levelized cost of energy (LCOE) is used to analyze and compare the economic performance of PTR and PTR-RS.

3.2.1 Initial investment

The initial investment mainly includes the ground field (site improvements), solar field, thermal storage,

HTF, power block, and fossil/heater backup [39]. Solar field cost and HTF cost refer to the cost per square meter of the solar field area to account for expenses related to installation of the solar field, and related to installation of the pumps and piping, respectively. Obviously, the costs of the solar field respectively employing the PTR and PTR-RS are different, the manufacturing cost of PTR-RS is approximately 10 % higher than that of the PTR according to the real manufacturing experience.

Thermal storage cost means the cost per thermal kilowatt (kWt) of storage capacity to account for expenses related to the installation of the thermal storage system. The power block cost is the cost per electric kilowatt (kWe) of power block gross capacity to account for the installation of the power block. It is worth noting that all of the costs mentioned above include the labor and equipment costs. The fossil/heater backup is necessary equipment for the CSP plants to compensate for the heat losses of the HTF to avoid the lower temperature and even freezing in the nighttime and off-hours of the solar field. According to the empirical PTCSP plant, the detailed costs used to calculate the initial investment cost of the plant are presented in the Table 2.

Table 2 Initial investment cost [40, 31]

Initial investment category	**Unit cost**
Ground field	25 \$/m^2 (Land area)
Solar field with the PTR/PTR-RS	150 / 152.5 \$/m^2 (Collector aperture area)
HTF system	60 \$/m^2
Thermal storage	62 \$/kWt
Power block	910 \$/kWe
Fossil/Heater backup	30 \$/kWe

3.2.2 Operation and maintenance costs

Operation and maintenance costs refer to the annual expenses on equipment and services occurring in the operation of the plant system. In this study, the average fixed operation and maintenance costs mainly consist of fixed cost by capacity, variable cost by generation, and insurance expense. The fixed cost by capacity and variable cost by generation can be determined as 66 $/kW-year and 4 $/MWh, respectively [41]. The insurance expense can be calculated by the expression as follows,

Insurance expense in *Year n*=Total installed Costs ($)×insurance rate (%)×(1+inflation rate)$^{n-1}$, (14)

where insurance rate and inflation rate are set as 0.5 and 2.5 %. Assumed that the analysis period of the PTCSP is 25 years in this study, annual operation and maintenance cost can be obtained. For a 100 MWe PTCSP plant with thermal storage for 6 hours, the average annual operation and maintenance cost is calculated as around 14 million dollars. The detailed results are presented in section 4.2.

3.2.3 Levelized cost of energy (LCOE)

The levelized cost of energy (LCOE) is a useful metric for the economic comparison between the different PTCSP plants. Absolutely, lower value of LCOE means better economic performance achieved by the PTCSP plant.

Assuming that the operating lifetime of the PTCSP plant is 25 years, the LCOE can be calculated by the Eq as follows [42]:

$$LCOE = \frac{I_0 + (\sum_{i=1}^{j} I_i + OM_i + FH_i)/(1+d)^i}{(\sum_{i=1}^{j} E_i)/(1+d)^i}, \quad (15)$$

where I_0 refers to the initial investment, I_i, OM_i, and FH_i are the investment expenditures, operation and maintenance expenditures, and fossil/heater expenditures in the year i, respectively. E_i is the electricity generated by the PTCSP system in the year i. j is the lifetime of the system. d is the discount rate which refers to the interest rate used in discounted cash flow analysis to determine the present value of future cash flows

[43, 39]; its value is 6.4 % in this study.

3.3 Experimental validation

In the previous study [29], the indoor heat loss and outdoor thermal efficiency experiments (Fig. 7(a)(b)) were carried out, and the experimental results were analyzed in detail. The indoor heat losses in PTR and PTR-RS under different absorber temperatures are presented in Fig. 8. The relational expressions of the curves fitting the discrete experimental data of the PTR and PTR-RS are:

$$HL_{PTR} = 0.1598T_s + 6.23\bullet10^{-9}T_s^4, \tag{16}$$

$$HL_{PTR-RS} = 0.1566T_s + 4.45\bullet10^{-9}T_s^4. \tag{17}$$

Obviously, it can be observed from Fig. 8 that RS plays a significantly positive role in reducing solar receiver heat loss since the RS could effectively block the radiation heat loss from the absorber tube. The amount of heat loss blocked by RS in PTR-RS compared to PTR increases at higher absorber temperature. It is because, with the higher absorber temperature, the absorber tube will emit a larger amount of radiation heat loss, the RS will be accordingly more efficient for interception of radiation heat loss. When the absorber temperature is 550 °C, the total heat loss of PTR-RS and PTR are 493.3 and 658.0 W/m, respectively. The heat loss of the former is effectively reduced by 25.0% compared with that of the latter.

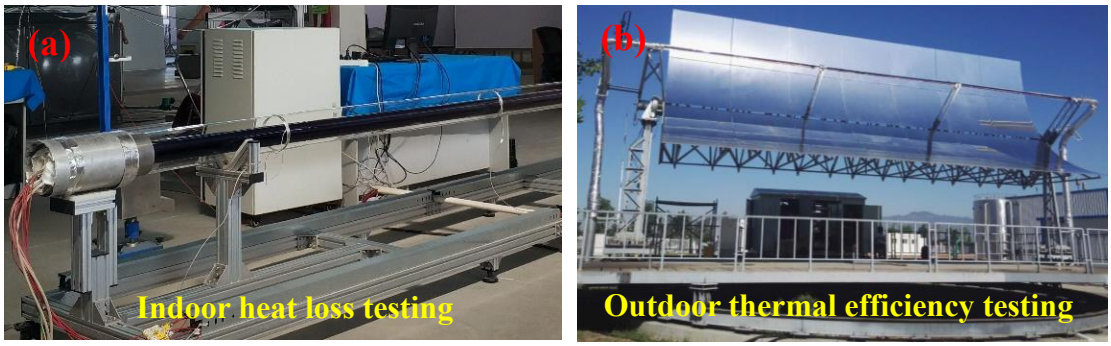

Fig. 7 Indoor and outdoor experimental testing

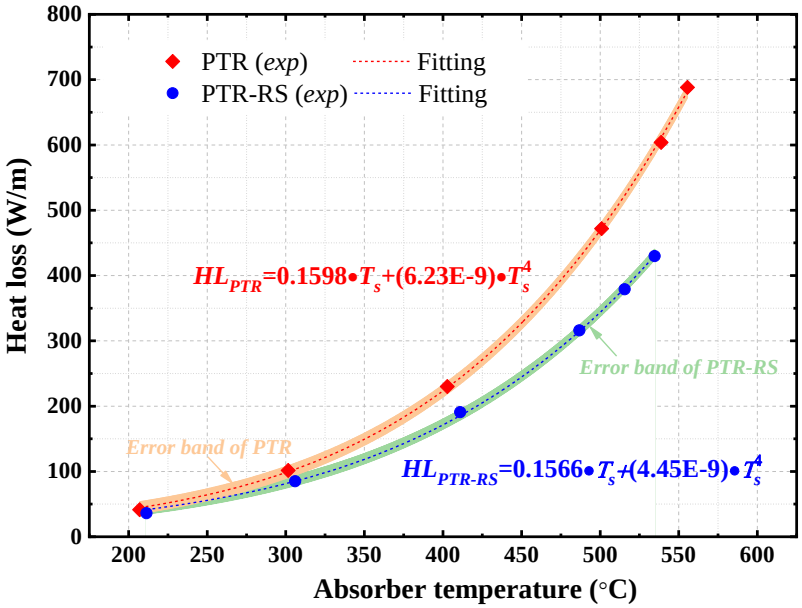

Fig. 8 The experimental results in the indoor heat loss testing

In the outdoor experiments, the PTC testing platform used the silicone oil as the HTF. The length and aperture width of the PTC testing platform are 12 and 5.76 m, respectively. The platform can rotate horizontally in a circular orbit, thus realizing double-axis tracking. Based on the heat loss data achieved by the Eq (10) and (11), the thermal efficiency of the PTC system is simulated according to the model in section 3.1. The operating and environmental parameters used in the simulation model are the same as these in the outdoor experiments . In this study, the root-mean-square deviation (*RMSD*) is employed to evaluate the consistency between simulated results and experimental data, and it is expressed as [44]:

$$RMSD = \sqrt{\frac{\sum[(X_{sim,i} - X_{\exp,i}) / X_{\exp,i}]^2}{n}}, \tag{18}$$

where the X_{sim} and X_{exp} refer to the simulated data and experimental data, respectively. n is the number of data. The simulated and experimental results are shown in Fig. 9. It is obviously observed that the simulated thermal efficiency curves of PTR and PTR-RS have good consistency with the fitting curves of the experimental results. It is calculated that the values of *RMSD* for the PTR and PTR-RS remain within 4.5 %, which demonstrates that the established model has satisfactory ability to predict the thermal performance of the PTR and PTR-RS in the PTCSP system with precision.

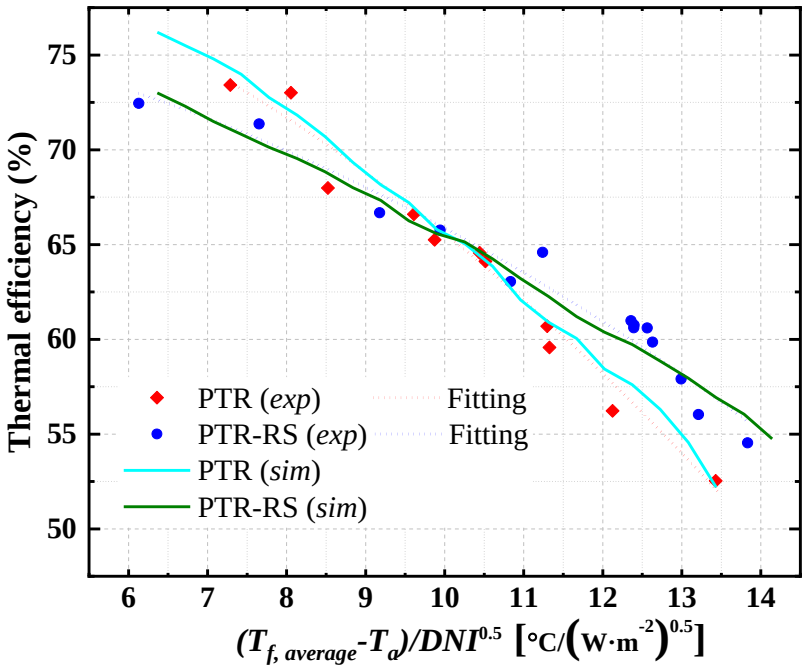

Fig. 9 The comparison between the experimental and modeled results

4. Results and discussion

4.1 Overall thermal performance of PTR-RS in the PTCSP plant

To investigate the overall thermal performance of the proposed PTR-RS, the solar receivers of PTRs and PTR-RSs are respectively employed to the 100 MWe PTCSP plants with thermal storages for 6 hours. In a single loop, the HTF temperature flowing inside of solar receivers gradually increases from the low inlet temperature of 290 °C to the desired high outlet temperature of 550 °C through a solar field loop. The mass flow rate of the HTF is accurately adjusted to obtain the desired operating temperature at the outlet of the loop according to the value of *DNI*, thereby the HTF temperatures along with the single loop are almost identical for the PTR and PTR-RS under different values of *DNI*.

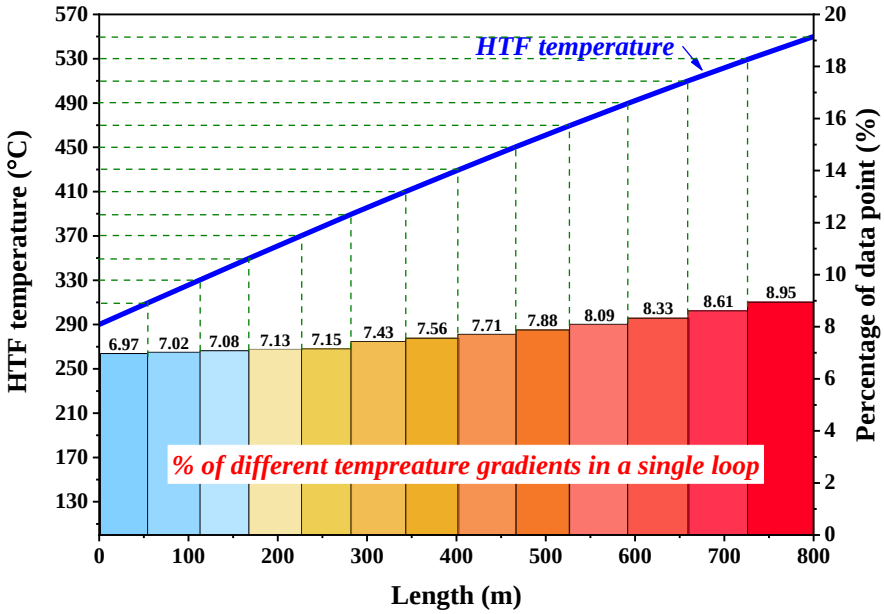

Fig. 10 HTF temperatures along with the single loop

The HTF temperatures increasing gradually along with the single loop are exhibited in Fig. 10. The temperature difference of 260 °C between the inlet and out temperatures are divided into 13 temperature gradients on average with an interval of 20 °C, and the percentages of different temperature gradients accounting for the loop length are also presented in Fig. 10. It is observed that the HTF temperature increases fast in the lower temperature gradients, for example, the HTF temperature rising process from 290 to 310 °C is complemented in just 6.97% of total loop length, i.e., approximately 55.8 m. In the higher temperature gradients, however, the growth rate of HTF temperature becomes slow, the corresponding percentages of the higher temperature gradients in a single loop increase. For instance, the last temperature gradient from 530 to 550 °C is achieved by 8.95% of the total loop length, about 71.6 m. All of the observations above demonstrate that the growth rate of HTF temperature along with the loop would be slower with the increasing temperature. This is because the thermal efficiency of the solar receiver at higher operating temperature decreases since the massive amount of heat loss of the solar receiver occurs at such temperature. This characteristic of HTF temperature along with the loop results in a higher average HTF temperature of 425.6 °C in a loop, which is conducive to use the proposed PTR-RS in the solar field to effectively reduce the total heat loss of the loop.

To more intuitively compare the overall thermal performance of the PTR and PTR-RS, the loop heat loss and loop thermal efficiency are investigated as shown in Fig. 11 and Fig. 12. In the daytime or service hours of the solar field, the heat loss of a single loop using the PTR-RSs as the solar receivers is effectively reduced by 23.6% compared with the PTRs. In the nighttime or off-hours of the solar field, the HTF temperature is heated by electricity or fossil to maintain above 270 °C for preventing the freezing of solar salt. Assuming that the average HTF temperature is about 280 °C in the nighttime, the PTR at such a high temperature in the nighttime still emit much heat loss to the environment. Compared with the PTR, the RS in the PTR-RS can continue to play an effective role in intercepting the radiation heat loss from the absorber tube. Different from daytime, moreover, the RS doesn't block the incident solar irradiance because of no solar irradiance in the nighttime. Therefore, the RS would exert greatly positive impacts on the reduction of the heat loss of the PTR-RS in the nighttime. As shown in Fig. 11, the nominal loop heat loss of the PTR-RSs is calculated to be reduced by 14.3% in comparison with the PTRs. These demonstrate that the PTR-RSs can play an effective role in the heat loss reduction of the solar field not only in the daytime but also in the nighttime, which contributes to the enhancement of the utilization value of the PTR-RS in the PTCSP plant.

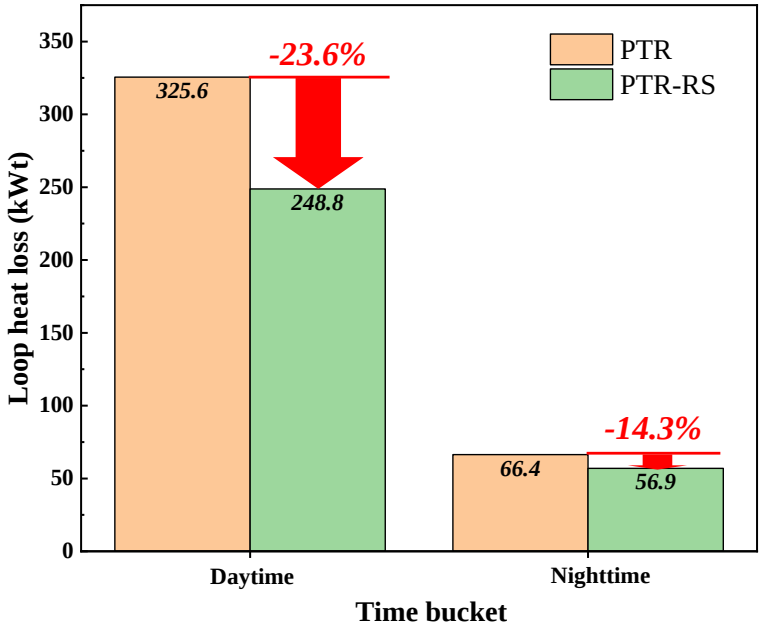

Fig. 11 Loop heat losses of PTR and PTR-RS in the daytime and nighttime

The *ANI*, which depends on the *DNI* and incidence angle according to Eq (2), has a vital impact on the performance of PTR-RS. As shown in Fig. 12, the loop thermal efficiencies of the PTR-RS are apparently higher than these of the PTR under lower *ANI*, the maximum enhancement percentage of 5.8 % occurs at the *ANI* of 300 W/m^2 where the loop thermal efficiencies of the PTR-RS and PTR are 60.3 and 57.0%, respectively. Correspondingly, the loop mass flow rate of the PTR-RS increases to 2.3 kg/s compared to 2.1 kg/s of the PTR. With the increasing *ANI*, the gaps in the thermal efficiency and mass flow rate between the PTR and PTR-RS gradually lower, their thermal efficiencies and mass flow rates are almost the same at the *ANI* of 1000 W/m^2. These phenomena appear because the presence of RS in the PTR-RS incurs limited solar irradiance loss which is much lower than the radiation heat loss blocked by the RS under lower *DNI*, thereby the PTR-RS possesses superior thermal efficiency. However, the solar irradiance loss incurred by the RS increases and approaches the radiation heat loss blocked with the growing DNI, leading to less effectiveness of the RS and less performance enhancement of the PTR-RS.

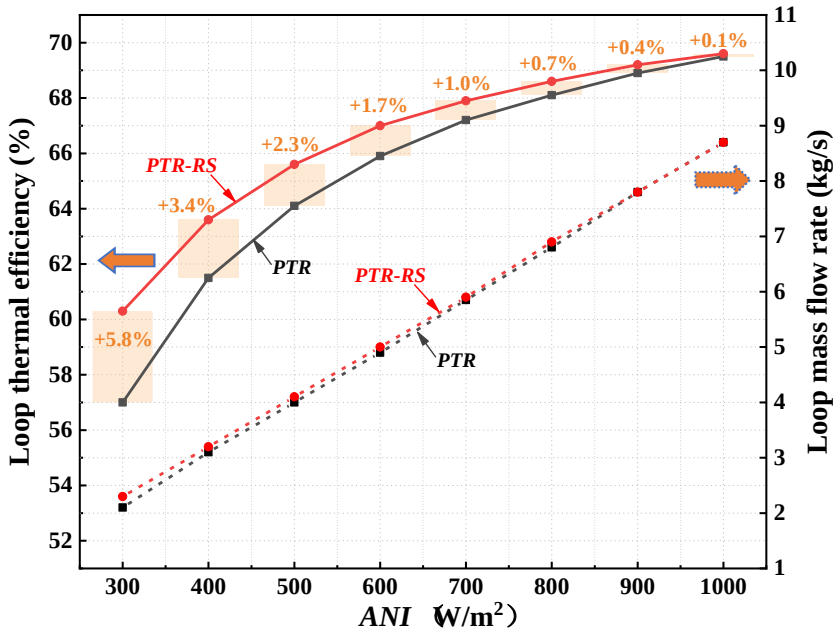

Fig. 12 Loop thermal efficiencies and mass flow rates of PTR and PTR-RS

The detailed metrics of the PTCSP plants with the PTRs and PTR-RSs are presented in Table 3. Assuming that the nominal *ANI* is 600 W/m^2, the loop thermal efficiencies of the PTR and PTR-RS are 65.9 and 67.0 %,

respectively. Due to a superior thermal efficiency achieved by the PTR-RS, the thermal power output of single loop in the PTCSP plant with the PTR-RSs is larger than that with the PTRs. Accordingly, the needed number of loops for the PTCSP plant with the PTR-RSs is smaller than that with the PTRs, which is much conductive to save the investment cost of the plant. Besides, the lower heat loss of PTR-RS in the nighttime shows great potential to save the fossil or electricity used to prevent field freeze.

Table 3 Metrics of solar fields in the PTCSP plants with the PTRs and PTR-RSs

Metric	PTCSP plant with the PTRs	PTCSP plant with the PTR-RSs
Thermal power of power cycle (MWt)	245.7	
Turbine efficiency of power cycle (%)	40.7	
Nominal *ANI* (W/m^2)	600	
Loop thermal efficiency (%)	65.9	67.0
Loop mass flow rate (kg/s)	4.9	5.0
Loop thermal power (MWt)	1.72	1.75
Number of loops	285	281
Total aperture area of solar field (m^2)	1242600	1225160
Nominal field freeze protection (kWe)	19920	16830

4.2 Techno-economic assessments on the PTCSP plants in different areas

To verify the real performance of the PTCSP plants with different solar receivers, three typical areas, namely, Mojave desert, Quarzazate, and Dunhuang, are investigated in this section [45-47], the detailed weather data of three areas is presented in Table 4 [48, 49]. Mojave desert and Dunhuang have the best and worst *DNI* sources among three typical areas, the annual total *DNIs* of Mojave desert, Quarzazate, and Dunhuang are 2777.7, 2219.2, and 1982.0 kWh/(m^2·y), respectively. The exact hourly values of *DNI* and *ANI*

on the aperture plane of SCAs in three areas are shown in Fig. 13. The average values of *DNI* in these three areas are calculated as 623.8, 500.4, and 445.1 W/m^2.

Table 4 Weather data of three typical areas

Area	Location	Annual total *DNI* (kWh/(m^2·y))	Average ambient temperature (°C)	Average wind speed (m/s)
Mojave Desert	(106.78°W, 32.37°N), USA	2777.7	16.7	2.7
Quarzazate	(6.90°W, 30.94°N), Morocco	2219.2	20.1	2.4
Dunhuang	(94.68°E, 40.15°N), China	1982.0	11.0	2.1

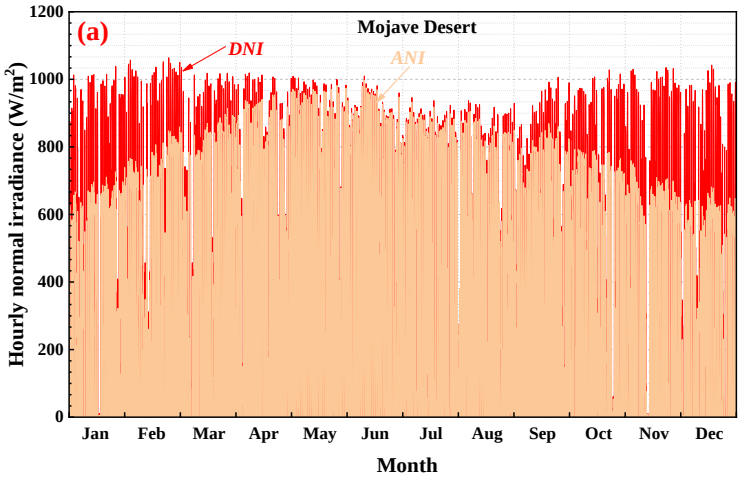

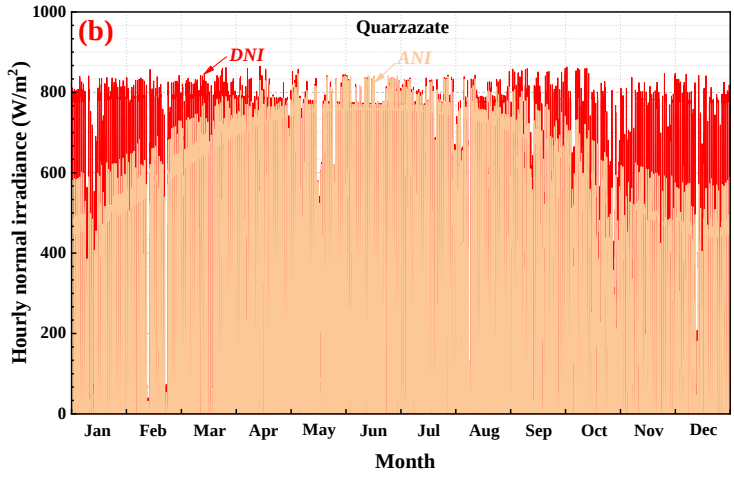

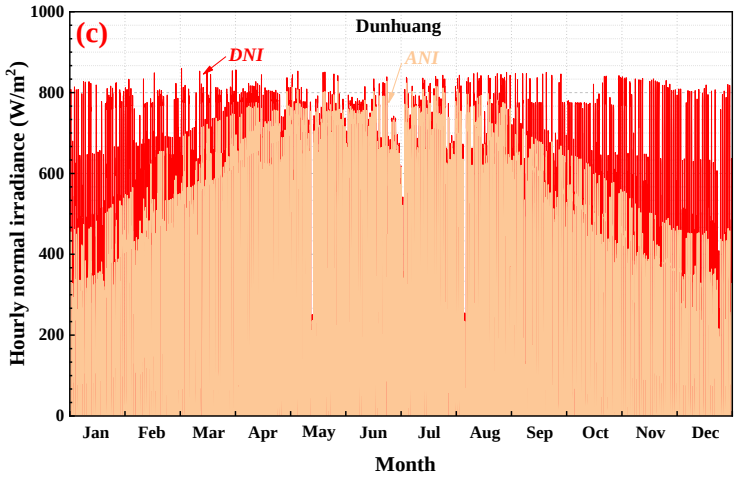

Fig. 13 Hourly *DNI* and *ANI* in three typical areas, namely, (a) Mojave desert, (b) Quarzazate, and (c) Dunhuang.

The detailed techno-economic metrics of 100 MWe PTCSP plants (thermal storage for 6 hours) with the PTRs and PTR-RSs are presented in Table 5. It is observed that the PTCSP plants with the PTR-RSs in three areas exhibit great enhancements of electrical energy production compared with these with the PTRs, the relative percentages (*RP*s) of the enhancements of annual net electrical energy productions in these three areas are 5.61, 7.16, and 9.77 %, which proves again that the PTR-RS exerts a more effective role in the area with lower *DNI*. The freeze protections mainly consist of thermal storage freeze protection and solar field freeze protection. Due to long loops in the solar field, the heat loss escaping from the PTRs in the solar field is much more considerable than the storage tank with good insulation. Thus, the energy consumption used to protect the solar field freeze accounts, to an overwhelming extent, for most of the total freeze protections by the data comparisons in Table 5. As explained in Fig. 11, the RS could effectively reduce the heat loss in the PTR-RS without incurring solar irradiance loss at the nighttime. Promisingly, the utilization of the PTR-RSs in the PTCSP plant can greatly reduce the energy consumption for the field freeze protection by above 36.0 %. Due to the increases of material and manufacture costs of RS in the PTR-RS, the initial investment costs of the PTCSP plants with the PTR-RSs increase by 0.07% in three areas. Besides, the average annual operation and maintenance (OM) costs of the PTCSP plants with the PTR-RSs also grow by 0.82~1.01% in three areas.

Though the initial investment cost and OM costs increase in the PTCSP with the PTR-RSs, the enhanced annual electrical energy production can fully offset these additional costs, and the real LCOE values are significantly reduced in these three areas. The real LCOE of the PTCSP plant with the PTR-RSs in the Dunhuang is reduced by 8.67 % from 13.50 cent/kWh in the plant with the PTRs to 12.33 cent/kWh, the relative reduction percentages of the real LCOE in the Quarzazate and Mojave desert are 6.33 and 5.03 %, respectively. The assessments above show that the PTR-RS has great potentials to enhance the techno-economic performance of the PTCSP plant in different areas of the world.

Table 5 Metrics in the PTCSP plants with the PTRs and PTR-RSs (100 MWe, thermal storage for 6 hours) in three areas

Metrics	Mojave desert			Quarzazate			Dunhuang		
	PTR	**PTR-RS**	***RP* (%)**	**PTR**	**PTR-RS**	***RP* (%)**	**PTR**	**PTR-RS**	***RP* (%)**
Annual net electrical energy production (MWhe)	387889.63	409632.64	+5.61	340652.16	365028.26	+7.16	265040.83	290945.73	+9.77
Annual freeze protection (MWhe)	39100.01	24086.82	-38.40	39893.12	25365.73	-36.42	42261.10	27050.82	-35.99
Annual field freeze protection (MWhe)	39067.86	24077.16	-38.37	39728.82	25295.62	-36.33	41538.5	26320.56	-36.64
Initial investment cost ($1m)	529.98	530.34	+0.07	530.00	530.36	+0.07	530.05	530.40	+0.07
Average annual operation and maintenance costs ($1m)	14.59	14.71	+0.82	14.33	14.47	+0.98	13.92	14.06	+1.01
Real LCOE (¢ /kWh)	9.34	8.87	-5.03	10.58	9.91	-6.33	13.50	12.33	-8.67

4.3 Parametric analysis on the PTR-RS in the PTCSP plant

4.3.1 Installed capacity of PTCSP plant

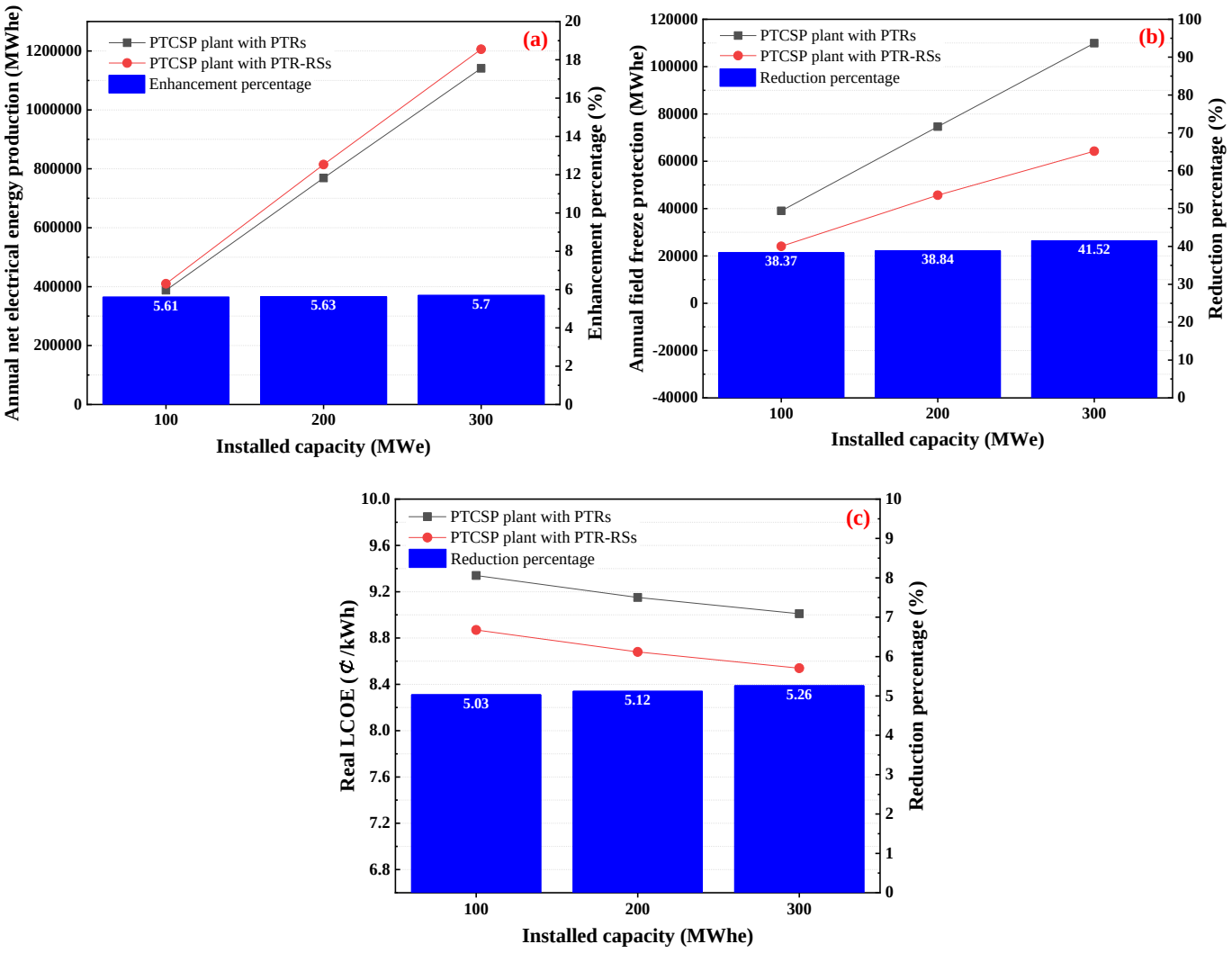

Fig. 14 Metrics of PTCSP plants (thermal storage for 6 hours) in the Mojave desert with different installed capacity

Larger installed capacity of the PTCSP plant means a larger solar field to collect more solar energy, the techno-economic performance of the PTCSP would accordingly fluctuate. In this section, three PTCSP plants located in the Mojave desert with the installed capacities of 100, 200, and 300 MWe are investigated. The calculation results are exhibited in Fig. 14. With the increasing installed capacity, the annual net electrical energy productions (Fig. 14(a)) and the annual field freeze protection (Fig. 14(b)) of the PTCSP plants with the PTRs and PTR-RSs have significant increases. The enhancement percentages of the annual net electrical energy production of the former have smaller variations under different installed capacities compared with

that of the latter, maintaining around 5.60 %. Due to the enlarged solar field, the PTR-RSs play more dramatic roles in reducing the field freeze protection in the PTCSP with higher installed capacity. In the PTCSP plant with the installed capacity of 300 MWe, the reduction percentage of annual field freeze protection of the PTR-RSs reaches 41.52 % compared with that of the PTRs. The real LCOE results in Fig. 14(c) show that the real LCOEs of PTCSP plants with PTRs and PTR-RSs decreases with higher installed capacity due to the reducing equipment and construction costs in a larger-scale plant, in addition, the PTCSP plant with the PTR-RSs under higher installed capacity possesses better economic performance. The real LCOE values of the PTCSP plants with the PTRs and PTR-RSs under the installed capacity of 300 MWe are 9.01 and 8.54 cents/kWhe, the reduction percentage of the latter reaches 5.26 % in comparison to the former.

4.3.2 Thermal storage capacity

The thermal storage capacity, i.e., full-load storage hours, is another important parameter in the PTCSP plant. A longer hour of thermal storage will increase the annual net electrical energy production and the construction cost, which can be proven in Fig. 15(a) and (b). Comparing the metrics of the PTCSP plant installing the PTR-RSs with these installing the PTRs, the enhancement percentages of annual net electrical energy production in the former plant increase slightly with the larger thermal storage capacity. Therefore, larger thermal storage capacity contributes to a more effective role in improving the electrical energy production of the plant exerted by the performance-enhanced PTR-RSs. Different from the energy production, the additional initial investment cost in the PTCSP plant with the PTR-RSs is relatively reduced from 0.07 to 0.06 % compared to the plant with the PTR, this is because the account of the investment cost in the thermal storage for the total investment cost increases with larger thermal storage capacity, that results in the reduced account of the investment cost in the solar field for the total investment cost in the PTCSP plant.

The real LCOE values of the PTCSP plants under different thermal storage hours are presented in Fig.

15(c). In a CSP plant, the LCOE mainly depends on CSP installed capacity, the investments of solar field and storage tanks, and the local solar irradiance source. Under the determined installed capacity of 100 MWe in this study, larger storage hour means more electricity production, which could bring more revenue; simultaneously, it also means a larger-scale solar field and storage tank required, which causes more initial investments of the solar field and storage tanks. It is observed that the LCOE values of the PTCSP plants go down and then up with the increasing thermal storage hours. The reason for this situation is that additional revenue of the enhanced electrical energy production of the PTCSP plant is over additional investment cost on the thermal storage and solar field when the thermal storage hours are raised from 6 to 8 hours, but the relationship will reverse when the storage hour is further raised to 10 hours. Therefore, the optimum storage hour could happen near 8 hours with a high possibility. Besides, the comparisons of the LCOE values between the plant with PTRs and that with PTR-RSs show that, the LCOE value in the latter is reduced more effectively at longer thermal storage hours, the reduction percentage reaches 5.15 % in the PTCSP plant with the thermal storage for 10 hours.

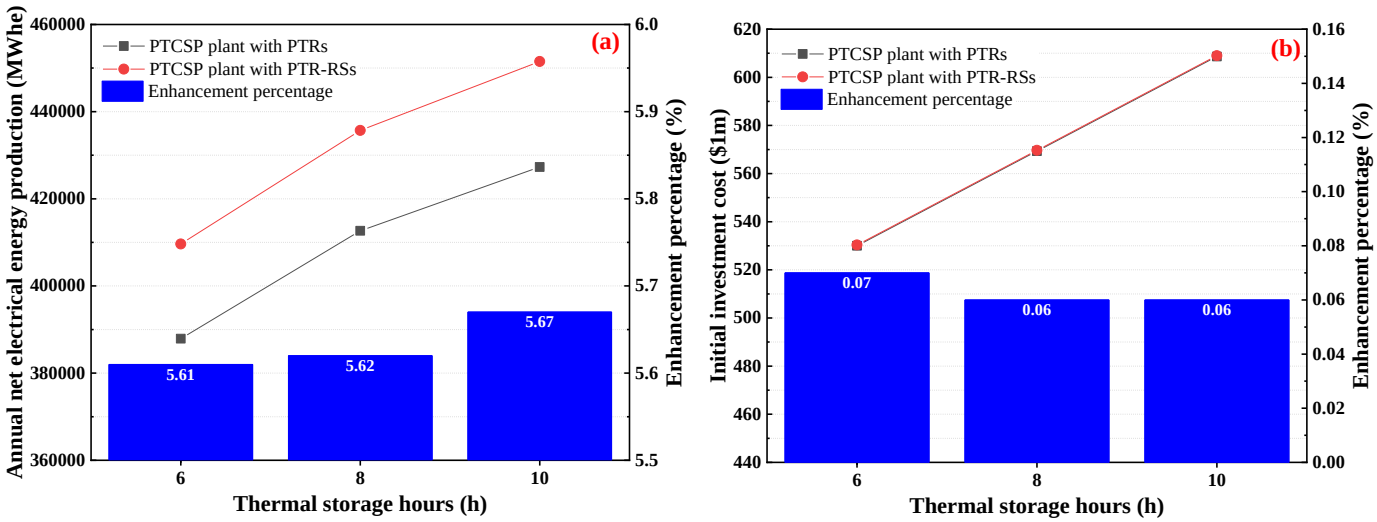

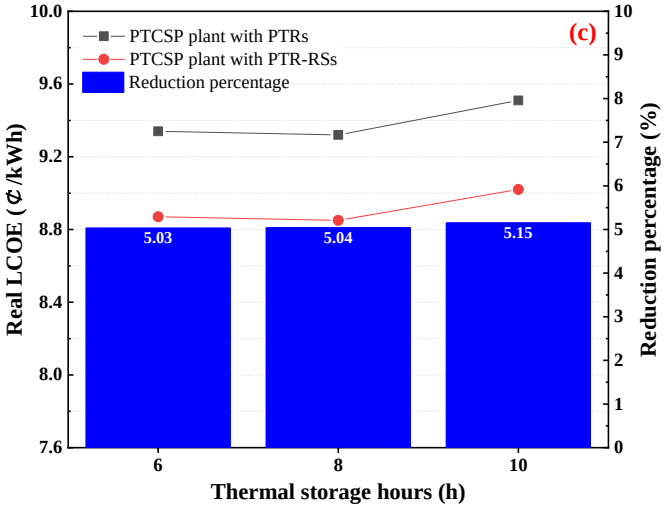

Fig. 15 Metrics of PTCSP plants (installed capacity of 100 MWe) in the Mojave desert with different thermal storage capacities

5. Conclusions

Based on the theory of the negative thermal-flux region, a novel parabolic trough receiver with a radiation shield (PTR-RS) was proposed to effectively reduce the heat loss and improve the solar-to-thermal conversion performance of the PTC system. To further verify the feasibility of the proposed PTR-RS in the PTCSP plant under the real environmental conditions, the overall techno-economic performance of the PTR-RSs in PTCSP plants using the solar binary salt as the HTF is investigated in this study. The mathematical model established is validated, and the simulation results exhibit satisfactory consistencies with the experimental data. The results demonstrate that the PTR-RS has great potential for the effective enhancements of the techno-economic performance of the power plant. The results are summarized as follows:

(1) The PTR-RS plays an effective role in the heat loss reduction of the solar field not only in the daytime but also in the nighttime. Besides, the loop thermal efficiency of the PTR-RS in the solar field with nominal outlet fluid temperature of 550 ℃ is apparently higher than that of the PTR. The relative enhancement percentage of loop thermal efficiency reaches 5.8-0.1 % at the normal irradiance of 300-800 W/m^2.

(2) The PTCSP plant installing PTR-RSs has the best effect of the enhancements of techno-economic performance in Dunhuang with a lower *DNI* in comparison with these in Mojave desert and Quarzazate. The

PTCSP plant with the PTR-RSs located in Dunhuang can effectively improve the annual net electrical energy production by 9.77 %, reduce the annual field freeze protection and LCOE by 36.64 and 8.67 %, respectively.

(3) Larger enhancements of the electrical energy production and more effective reductions of the LCOE are achieved by the PTCSP plant installing the PTR-RSs with the increasing installed capacity and thermal storage capacity. These demonstrate the great feasibility of the PTR-RS in the PTCSP plant.

Acknowledgments

This study was sponsored by the RGC Postdoctoral Fellowship Scheme 2020/2021 (3-RA59) and the Postdoctoral Hub program (PiH/160/19) of the Innovation and Technology Fund of the Hong Kong SAR Government, and the National Science Foundation of China (51761145109, 51776193).

References

[1] Caccia M, Tabandeh-Khorshid M, Itskos G, et al. Ceramic–metal composites for heat exchangers in concentrated solar power plants. Nature 2018; 562(7727): 406-409.

[2] González-Roubaud E, Pérez-Osorio D, Prieto C. Review of commercial thermal energy storage in concentrated solar power plants: Steam vs. molten salts. Renewable and sustainable energy reviews 2017; 80: 133-148.

[3] Fernández A G, Gomez-Vidal J, Oró E, et al. Mainstreaming commercial CSP systems: A technology review. Renewable Energy 2019; 140: 152-176.

[4] Li G, Xuan Q, Akram M W, et al. Building integrated solar concentrating systems: A review. Applied Energy 2020; 260: 114288.

[5] Wang K, Li M J, Zhang Z D, et al. Evaluation of alternative eutectic salt as heat transfer fluid for solar power tower coupling a supercritical CO_2 Brayton cycle from the viewpoint of system-level analysis. Journal of Cleaner Production, 279: 123472.

[6] Bellos E, Tzivanidis C. Alternative designs of parabolic trough solar collectors. Progress in Energy and Combustion Science 2019; 71: 81-117.

[7] Fuqiang W, Ziming C, Jianyu T, et al. Progress in concentrated solar power technology with parabolic trough collector system: A comprehensive review. Renewable and Sustainable Energy Reviews 2017; 79: 1314-1328.

[8] Wang K, Zhang Z D, Li M J, et al. A coupled optical-thermal-fluid-mechanical analysis of parabolic trough solar receivers using supercritical CO2 as heat transfer fluid. Applied Thermal Engineering, 2020: 116154.

[9] Cheng Z D, Leng Y K, Men J J, et al. Numerical study on a novel parabolic trough solar receiver-reactor and a new control strategy for continuous and efficient hydrogen production. Applied Energy, 2020, 261: 114444。
[10] Hales D. Renewables 2020 global status report. Rep. Paris: REN21, 2020.
[11] Vignarooban K, Xu X, Arvay A, et al. Heat transfer fluids for concentrating solar power systems–a review. Applied Energy 2015; 146: 383-396.
[12] Bellos E, Tzivanidis C, Tsimpoukis D. Thermal, hydraulic and exergetic evaluation of a parabolic trough collector operating with thermal oil and molten salt based nanofluids. Energy conversion and management 2018; 156: 388-402.
[13] Maccari A, Bissi D, Casubolo G, et al. Archimede Solar Energy molten salt parabolic trough demo plant: a step ahead towards the new frontiers of CSP. Energy Procedia 2015; 69: 1643-1651.
[14] Burkholder F, Kutscher C. Heat loss testing of Schott's 2008 PTR70 parabolic trough receiver. National Renewable Energy Lab. (NREL), Golden, CO (United States), 2009.
[15] Wu Z, Li S, Yuan G, et al. Three-dimensional numerical study of heat transfer characteristics of parabolic trough receiver. Applied energy 2014; 113: 902-911.
[16] Wang Q, Yang H, Hu M, et al. Preliminary performance study of a high-temperature parabolic trough solar evacuated receiver with an inner transparent radiation shield. Solar Energy, 2018, 173: 640-650.
[17] Incropera F P, Lavine A S, Bergman T L, et al. Fundamentals of heat and mass transfer. Wiley, 2007.
[18] Coccia G, Di Nicola G, Sotte M. Design, manufacture, and test of a prototype for a parabolic trough collector for industrial process heat. Renewable energy 2015; 74: 727-736.
[19] Thappa S, Chauhan A, Sawhney A, et al. Thermal selective coatings and its enhancement characteristics for efficient power generation through parabolic trough collector (PTC). Clean Technologies and Environmental Policy 2020; 1-21.
[20] Rubin E B, Chen Y, Chen R. Optical properties and thermal stability of Cu spinel oxide nanoparticle solar absorber coatings. Solar Energy Materials and Solar Cells 2019; 195: 81-88.
[21] Osorio J D, Rivera-Alvarez A. Performance analysis of parabolic trough collectors with double glass envelope. Renewable energy 2019; 130: 1092-1107.
[22] McEnaney K, Weinstein L, Kraemer D, et al. Aerogel-based solar thermal receivers. Nano Energy 2017; 40: 180-186.
[23] Wang Q, Yang H, Hu M, et al. Optimization strategies and verifications of negative thermal-flux region occurring in parabolic trough solar receiver. Journal of Cleaner Production, 278: 123407.
[24] Wang Q, Yang H, Zhong S, et al. Quantitative analyses and a novel optimization strategy on negative energy-flow region in parabolic trough solar receivers. Solar Energy 2020; 196: 663-672.
[25] Yang H, Wang Q, Huang X, et al. Performance study and comparative analysis of traditional and double-selective-coated parabolic trough receivers. Energy 2018; 145: 206-216.
[26] Wang Q, Hu M, Yang H, et al. Performance evaluation and analyses of novel parabolic trough evacuated collector tubes with spectrum-selective glass envelope. Renewable energy 2019; 138: 793-804.
[27] Li Q, Zhang Y, Wen Z X, et al. An evacuated receiver partially insulated by a solar transparent aerogel for parabolic trough collector. Energy Conversion and Management 2020; 214: 112911.
[28] Qiu Y, Zhang Y, Li Q, et al. A novel parabolic trough receiver enhanced by integrating a transparent aerogel and wing-like mirrors. Applied Energy, 2020, 279: 115810.
[29] Wang Q, Yang H, Zhong S, et al. Comprehensive experimental testing and analysis on parabolic trough solar receiver integrated with radiation shield. Applied Energy 2020; 268: 115004.

[30] Fernández A G, Muñoz-Sánchez B, Nieto-Maestre J, et al. High temperature corrosion behavior on molten nitrate salt-based nanofluids for CSP plants. Renewable energy 2019; 130: 902-909.
[31] Delise T, Tizzoni A C, Menale C, et al. Technical and economic analysis of a CSP plant presenting a low freezing ternary mixture as storage and transfer fluid. Applied Energy 2020; 265: 114676.
[32] Al-Soud M S, Hrayshat E S. A 50 MW concentrating solar power plant for Jordan. Journal of Cleaner Production 2009; 17(6): 625-635.
[33] Denholm P, Mehos M. Enabling greater penetration of solar power via the use of CSP with thermal energy storage. Solar Energy: Application, Economics, and Public Perception 2014; 99.
[34] Aly A, Bernardos A, Fernandez-Peruchena C M, et al. Is Concentrated Solar Power (CSP) a feasible option for Sub-Saharan Africa? Investigating the techno-economic feasibility of CSP in Tanzania. Renewable energy 2019; 135: 1224-1240.
[35] Halimi M, Outana I, El Amrani A, et al. Prediction of captured solar energy for different orientations and tracking modes of a PTC system: Technical feasibility study (Case study: South eastern of MOROCCO). Energy Conversion and Management 2018; 167: 21-36.
[36] Padilla R V, Demirkaya G, Goswami D Y, et al. Heat transfer analysis of parabolic trough solar receiver. Applied Energy 2011; 88(12): 5097-5110.
[37] Gnielinski V. New equations for heat and mass transfer in turbulent pipe and channel flow. Int. Chem. Eng. 1976; 16(2): 359-368.
[38] Li G, Pei G, Su Y, et al. Performance study of a static low-concentration evacuated tube solar collector for medium-temperature applications. International Journal of Low-Carbon Technologies 2016; 11(3): 363-369.
[39] Blair N, Dobos A P, Freeman J, et al. System advisor model, sam 2014.1. 14: General description. National Renewable Energy Lab. (NREL), Golden, CO (United States), 2014.
[40] Islam M T, Huda N, Saidur R. Current energy mix and techno-economic analysis of concentrating solar power (CSP) technologies in Malaysia. Renewable energy 2019; 140: 789-806.
[41] Turchi, C. S. (2010). "Parabolic Trough Reference Plant for Cost Modeling with the Solar Advisor Model (SAM)," NREL/TP-550-47605.
[42] Shouman E R, Khattab N M. Future economic of concentrating solar power (CSP) for electricity generation in Egypt. Renewable and Sustainable Energy Reviews 2015; 41: 1119-1127.
[43] Carlin T M, Finch N, Schauten M, et al. The discount rate for discounted cash flow valuations of intangible assets. Managerial Finance, 2010.
[44] Hu M, Zhao B, Ao X, et al. Feasibility research on a double-covered hybrid photo-thermal and radiative sky cooling module. Solar Energy 2020; 197: 332-343.
[45] Skumanich A. CSP at a crossroads: The first solar electric power plants are still proving their worth after three decades, so why aren't we seeing more CSP reach the development stage. Renewable energy focus 2011; 12(1): 52-55.
[46] Mannah M A, Makki L, Haddad A, et al. Renewable Energy Technologies Penetration in MENA Region (2010-2030). Journal of Electrical Engineering 2016; 4: 100-107.
[47] Li R, Zhang H, Wang H, et al. Integrated hybrid life cycle assessment and contribution analysis for CO_2 emission and energy consumption of a concentrated solar power plant in China. Energy 2019; 174: 310-322.
[48] https://energyplus.net/weather.
[49] http://climate.onebuilding.org/default.html.